pISSN 1598-2998, eISSN 2005-9256

https://doi.org/10.4143/crt.2025.033 Cancer Res Treat. 2026;58(1):182-197

Original Article

Spatial Transcriptomic Landscape of Brain Metastases from Triple-Negative Breast Cancer: Comparison of Primary Tumor and Brain Metastases Using Spatial Analysis

Jihwan Yoo[1], **Inho Park**[2], **Hyun Jung Kim**[3], **Hun Ho Park**[1], **Sora Lee**[3], **Jee Hung Kim**[4,5], **Yoon Jin Cha**[2,5]

[1]Department of Neurosurgery, Brain Tumor Center, Gangnam Severance Hospital, Yonsei University College of Medicine, Seoul, [2]Department of Pathology, Gangnam Severance Hospital, Yonsei University College of Medicine, Seoul, [3]Department of Anatomy, Korea University College of Medicine, Seoul, [4]Department of Medical Oncology, Gangnam Severance Hospital, Yonsei University College of Medicine, Seoul, [5]Institute for Breast Cancer Precision Medicine, Yonsei University College of Medicine, Seoul, Korea

Purpose Triple-negative breast cancer (TNBC) is a particularly aggressive subtype of breast cancer, with approximately 30% of patients eventually developing brain metastases (BM), which result in poor outcomes. An understanding of the tumor microenvironment (TME) at both primary and metastatic sites offers insights into the mechanisms underlying BM and potential therapeutic targets.

Materials and Methods Spatial RNA sequencing (spRNA-seq) was performed on primary TNBC and paired BM tissues from three patients, one of whom had previously received immune checkpoint inhibitors before BM diagnosis. Specimen regions were categorized into tumor, proximal, and distal TME based on their spatial locations. Gene expression differences across these zones were analyzed, and immune cell infiltration was estimated using TIMER. A gene module analysis was conducted to identify key gene clusters associated with BM.

Results Distinct gene expression profiles were noted in the proximal and distal TMEs. In BM, the proximal TME exhibited neuronal gene expression, suggesting neuron-tumor interactions compared to tumor, and upregulation of epithelial genes compared to the distal TME. Immune cell analysis revealed dynamic changes in CD8+ T cells and macrophages across the tumor and TME zones. Gene module analysis identified five key modules, including one related to glycolysis, which correlated with patient survival. Drug repurposing analysis identified potential therapeutic targets, including *VEGFA*, *RAC1*, *EGLN3*, and *CAMK1D*.

Conclusion This study provides novel insights into the transcriptional landscapes in TNBC BM using spRNA-seq, emphasizing the role of neuron-tumor interactions and immune dynamics. These findings suggest new therapeutic strategies and underscore the importance of further research.

Key words Brain neoplasms, Triple-negative breast neoplasms, Spatial transcriptomics, Tumor microenvironment

Introduction

Brain metastases (BM) are the most prevalent type of brain tumor in adults, outnumbering primary brain tumors [1]. Common primary sites for BMs include lung, breast, melanoma, and renal cell carcinoma [2]. Among metastatic breast cancer patients, 30%-50% will develop BM during their illness, with prognosis and incidence varying according to the molecular subtype [3]. In triple-negative breast cancer (TNBC), roughly 30% of patients develop BM, generally experiencing poor clinical outcomes [3].

TNBC is defined by its lack of expression of estrogen receptor (ER) and progesterone receptor, along with non-amplified human epidermal growth factor receptor 2 (*HER2*) status. It represents an aggressive subtype of breast cancer, accounting for 10%-15% of all breast cancer cases [4]. In TNBC, mortality is chiefly associated with distant metastasis: the 5-year survival rate for localized disease is 91%, which declines to 12% upon development of distant metastasis [5]. Despite its aggressive nature, TNBC typically responds well to chemotherapy and immunotherapy, significantly affecting the long-term prognosis.

TNBC is considered the most immunogenic subtype among breast cancers and has attracted significant attention as a target for immunotherapy [6]. The level of tumor-infiltrating lymphocytes (TILs) is higher in TNBC compared to other subtypes. In the large-scale Breast International Group (BIG) 02-98 trial, the median percentage of tissue

Correspondence: Jee Hung Kim
Department of Medical Oncology, Gangnam Severance Hospital, Yonsei University College of Medicine, 211 Eonju-ro, Gangnam-gu, Seoul 06273, Korea
Tel: 82-2-2019-3305 E-mail: ok8504@yuhs.ac

Co-correspondence: Yoon Jin Cha
Department of Pathology, Gangnam Severance Hospital, Yonsei University College of Medicine, 211 Eonju-ro, Gangnam-gu, Seoul 06273, Korea
Tel: 82-2-2019-3540 E-mail: yooncha@yuhs.ac

Received January 8, 2025 **Accepted** April 13, 2025
Published Online April 15, 2025

*Jihwan Yoo, Inho Park, and Hyun Jung Kim contributed equally to this work.

area infiltrated by TILs was 20% in TNBC, compared to 15% in HER2-positive tumors and 10% in ER-positive, HER2-negative tumors [7]. Trials combining immune checkpoint inhibitor (ICI) targeting the programmed death protein 1 (PD-1) or programmed death-ligand 1 (PD-L1) in TNBC have shown benefits in some patients; however, the cancer and tumor microenvironment (TME) cell ecosystems have been minimally investigated [8-10]. Specifically, the distribution of immune cells in BM following ICI treatment holds significant implications for the future treatment of metastatic breast cancer [11]. As functional immune statuses and tumor characteristics in BM are expected to differ from those in the primary tumor, spatially resolved analysis would provide a more comprehensive understanding of BM.

Recent advances in spatial RNA sequencing (spRNA-seq) have enabled comprehensive analysis of tumors and their surrounding microenvironment by quantifying spatially resolved mRNA expressions. Unlike single-cell RNA sequencing (scRNA-seq), which lacks spatial context, spRNA-seq offers valuable insights into gene expression landscapes by analyzing tumors at the tissue level. In this study, we aimed to dissect the spatial architecture of TNBC and paired BM by compartmentalizing tumor regions and analyzing the TME to assess the genomic status of each region.

Materials and Methods

1. Specimen preparation

Between 2015 and 2022, three TNBC patients with available tissue from primary breast cancer (PC) and corresponding BM were selected at Gangnam Severance Hospital. All three patients underwent neoadjuvant chemotherapy for PC, developed BM post-mastectomy, and subsequently had surgical removal of the BM. The disease course for each patient is depicted in Fig. 1. Clinical data, including age at diagnosis, the interval between breast surgery and BM onset, treatment regimens, and responses, were extracted from the electronic medical records (Table 1).

Histopathologic assessments, such as nuclear grade, histologic grade, and triple-negative status, were conducted by a pathologist (YJC). For each patient, the most representative formalin-fixed paraffin-embedded (FFPE) blocks of one post-treatment residual TNBC and one BM were selected following a pathologic review. For each sample, a 10.5×10.5 mm section of FFPE tissue was cut to a thickness of 5 μm and mounted on a polarized slide for subsequent spatial transcriptomics analysis.

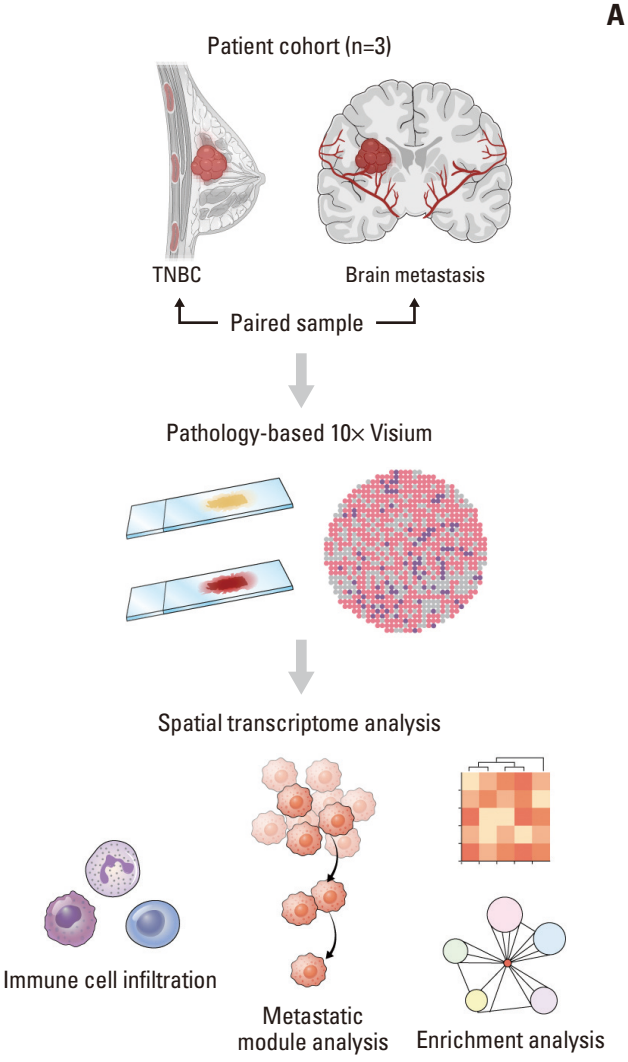

Fig. 1. Study design and clinical data of primary breast cancers paired with brain metastases. (A) Schematic diagram of the study, detailing the spatial transcriptome analysis conducted on paired samples (primary tumor and brain metastases) from three patients with triple-negative breast cancer (TNBC). *(Continued to the next page)*

2. Visium data analysis

To acquire whole transcriptome spatially barcoded sequence data from serial sections, we adhered to the Visium Spatial Gene Expression for FFPE protocol (Demonstrated Protocol CG000520). Tissue sectioning adhered to the Visium Spatial Gene Expression for FFPE – Tissue Preparation Guide (Demonstrated Protocol CG000518). The formalin-fixed, paraffin-embedded tissue samples were sectioned at 5 μm thickness and placed on Superfrost Plus Microscope Slides (Fisherbrand). The sections were then deparaffinized and stained with hematoxylin and eosin (H&E). After imaging, the sec-

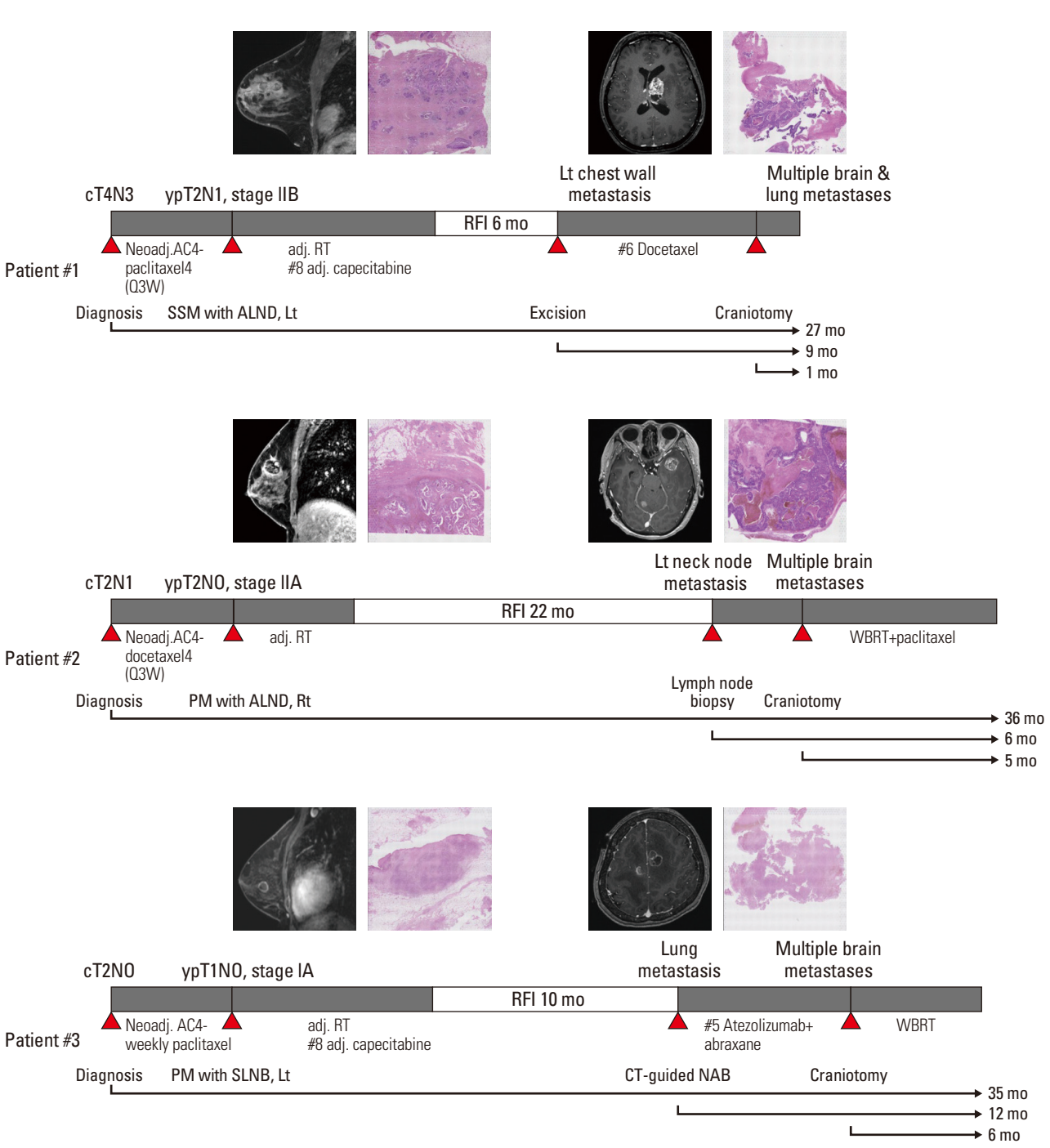

Fig. 1. *(Continued from the previous page)* (B) Collection of clinical samples, treatment process, and survival duration for each patient. AC, Adriamycin and cyclophosphamide; ALND, axillary lymph node dissection; CT, computed tomography; NAB, needle aspiration biopsy; Neoadj, neoadjuvant; PM, partial mastectomy; Q3W, once every 3 weeks; RFI, recurrence free interval; RT, radiotherapy; SLNB, sentinel lymph node biopsy; SSM, skin sparing mastectomy; WBRT, whole brain radiotherapy.

tions underwent decoverslipping, hematoxylin destaining, and decrosslinking.

The tissue sections were transferred to a Visium CytAssist Spatial Gene Expression slide using the Visium CytAssist instrument. This slide, featuring a capture area of 1.21 cm^2, facilitated analyte transfer. Following this, probe

Table 1. Baseline characteristics of the patients with triple-negative breast cancer

	Patient 1	Patient 2	Patient 3
Age at initial diagnosis (yr)	26	45	43
Histologic subtype	Invasive ductal carcinoma	Invasive ductal carcinoma	Invasive ductal carcinoma
Pathologic T category	2	2	1
Pathologic N category	1	0	0
Histologic grade	3	2	2
Ki67 labeling index (%)	50	70	47.20
PD-L1 (SP142)	0	0	IC 3% (positive)
PD-L1 (22C3)	0	0	CPS ≥ 10 (positive)
Neoadjuvant treatment	AC4-paclitaxel 4 (Q3W)	AC4-docetaxel 4 (Q3W)	AC4-weekly paclitaxel
RFI (mo)	6	22	10
Palliative systemic treatment (before brain metastasis)	Docetaxel	None	Atezolizumab+ Nab-paclitaxel

AC, Adriamycin and cyclophosphamide; CPS, combined proportional score; IC, immune cell; PD-L1, programmed death-ligand 1; Q3W, once every 3 weeks; RFI, recurrence free interval.

extension and library construction were conducted according to the Visium for FFPE standard workflow. Sequencing libraries were prepared using paired-end dual-indexing with settings of 28 cycles for Read 1, 10 cycles for i7 and i5 indices, and 90 cycles for Read 2. Libraries were demultiplexed using bcl2fastq (Illumina), and the resulting FASTQ files were analyzed using the Space Ranger pipeline v2.0.1 (10x Genomics) with the GRCh38-2020-A reference genome.

3. Pathologic annotation

Using Loupe Browser v6.2.0, pathologist (YJC) annotated paired PC and BM samples. For PC samples, tissue areas were categorized into six clusters based on their cellular structures: invasive carcinoma, ductal carcinoma *in situ* (DCIS), necrosis, tumor stroma, non-tumor stroma, and non-tumor epithelium.

Invasive carcinoma was characterized by infiltrating tumor epithelial cells that lacked surrounding myoepithelial cells. DCIS was identified by tumor epithelial cells confined within ducts and surrounded by myoepithelial cells. Necrotic areas, consisting of karyorrhectic cell debris typical of tumor necrosis, were annotated to be excluded from further analysis.

Tumor stroma was defined as the non-epithelial regions of the tumor tissue, including immune cells, mesenchymal cells, and vasculature constituting the TME. Non-tumor stroma included areas outside the tumor regions, devoid of epithelial components. Non-tumor epithelium comprised non-cancerous epithelial cells such as ductal and acinar cells from normal mammary glands adjacent to the tumor area on the same slide.

For BM samples, tissue areas were categorized into four clusters: metastatic carcinoma, non-epithelial tumor area, hemorrhage, and necrosis. For all three patients, glial tissue was not included in the specimens. Metastatic carcinoma encompassed the tumor epithelial cells of metastatic breast cancer. The non-epithelial tumor area consisted of regions of the metastatic tumor excluding the tumor epithelial cells. Necrosis and hemorrhage were annotated to segregate these compartments for analysis. The necrosis cluster contained tumor cell debris, and the hemorrhage cluster consisted of red blood cells.

4. Zone discrimination of specimen area by Visium data

To systematically analyze regional transcriptomics, we divided the peritumoral and non-tumor spots into two distinct distance zones, termed proximal TME and distal TME, respectively. We calculated the distances between the central coordinates of the peritumoral/non-tumor spots and tumor spots, as indicated by "pxl_row_in_fullres" and "pxl_col_in_fullres" from the tissue positions file. The diameter of each spot was 65 μm. The distance from each non-tumor spot to the nearest tumor spot was measured. Spots located within a predefined range 120 μm of tumor spots were defined as the proximal TME, corresponding to the peritumoral area, while spots located more than a specified distance 120 μm away from tumor spots were classified as the distal TME, representing the non-tumor neighboring area.

We conducted differentially expressing genes (DEGs) analysis using the FindMarkers() function in the Seurat package ver. 4.1.0 to generate the DEG list based on the regional categorization. With three zones (tumor, proximal TME, distal TME), three DEG lists were derived from the regional comparisons.

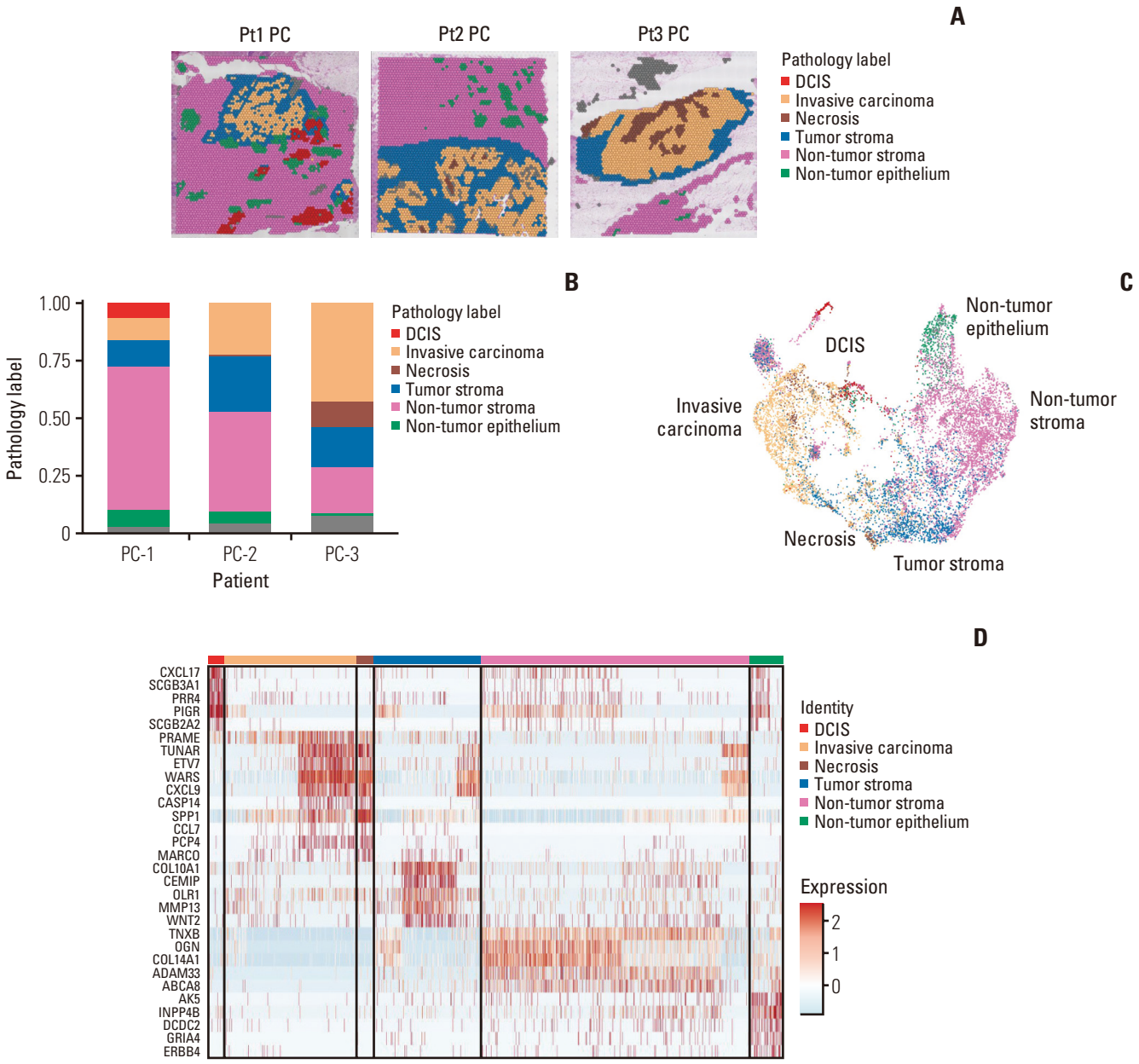

Fig. 2. Transcriptomic characterization of primary breast cancers and paired brain metastases. (A) Morphological regions in primary breast cancer (PC) were annotated by a pathologist into six distinct categories. (B) Proportions of spots assigned to each cluster across the three patients. Grey areas represent empty pixels where no tissue or cells were detected. (C) Uniform manifold approximation and projection (UMAP) embedding of all spots from the three patients, with markers colored based on pathological annotations. (D) A heatmap of the clusters displays the most highly differentially expressed genes, with colors representing normalized and scaled expression values. *(Continued to the next page)*

5. Cell deconvolution via TIMER

To calculate immune infiltration for each spot across the total of six Visium datasets, spot-specific count data was analyzed using TIMER 2.0 [12]. Among the various tools provided by TIMER 2.0, xCELL, which exhibited no missing values across all datasets, was utilized. The xCELL deconvolution technique facilitated the estimation of immune cell infiltration, including CD8+ T cells, CD4+ T cells, B cells, M1 macrophages and M2 macrophages in each spot. The estimated immune cell counts for each spot were then applied to the pathology slides for visualization. Furthermore, the immune cell estimations were categorized by zone and compared,

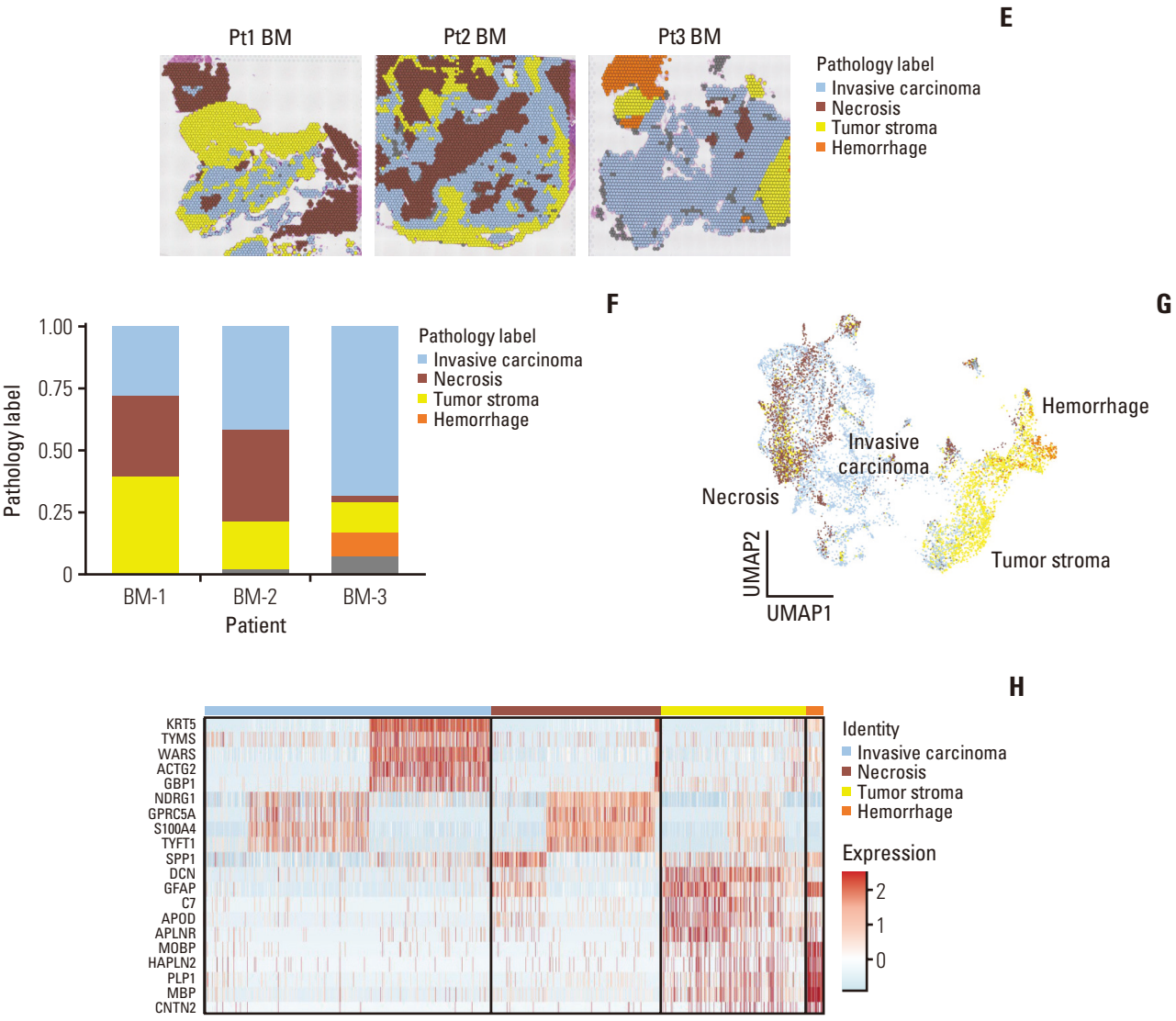

Fig. 2. *(Continued from the previous page)* (E) Morphological regions in brain metastases (BM) were annotated by a pathologist into four distinct categories. (F) Proportions of spots assigned to each cluster across the three patients. Grey areas represent empty pixels where no tissue or cells were detected. (G) UMAP embedding of all spots from the three patients, with markers colored based on pathological annotations. (H) A heatmap of the clusters shows the most highly differentially expressed genes, with colors representing normalized and scaled expression values. DCIS, ductal carcinoma *in situ*.

with the degree of increase evaluated for each patient.

6. Identification of relative modules across the samples

To identify the core transcriptional programs shared between PC and BM, we filtered out cancer cells from the integrated datasets and performed sub-clustering. Marker gene sets for each cluster were obtained using the FindAllMarkers function in the Seurat package. To ensure robust gene set clusters, shared genes between different clusters were excluded, and clusters with fewer than 50 genes were filtered out based on adjusted p-values < 0.05 and log2FC > 0.25. This process yielded 20 clusters, with 11 from BM samples and nine from PC samples. Expression scores for the relevant gene set were calculated using the AddModuleScore function in Seurat. Pearson correlation analysis was then conducted on the module scores for the 20 clusters, and the resulting matrix was utilized for hierarchical clustering with the ComplexHeatmap package. A correlation coefficient threshold of > 0.6 was employed to identify significant modules.

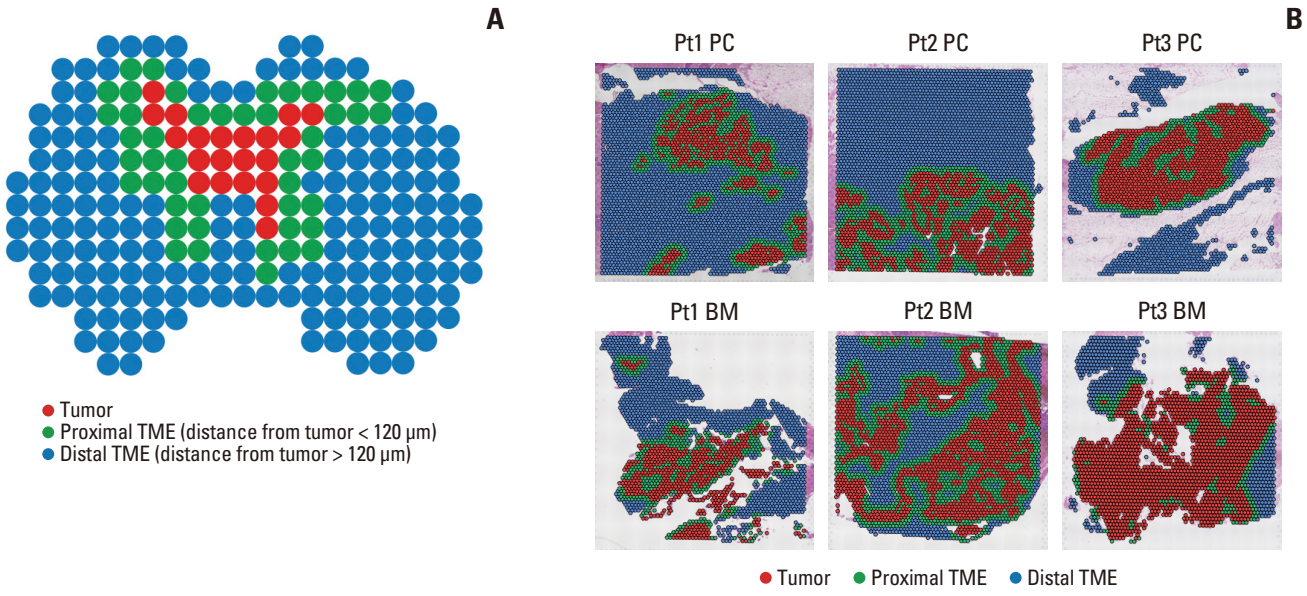

Fig. 3. Zonal categorization of the tumor microenvironment (TME). (A) Schematic diagram illustrating the definitions of TME, proximal TME, and distal TME. (B) A geographic representation of the samples, divided into three groups from three patients. BM, brain metastases; PC, primary breast cancer. *(Continued to the next page)*

7. Functional enrichment analysis

Enrichr was used to confirm the biological pathways associated with shared genes across the clusters in each module [13]. The shared genes, identified using the FindAllMarkers function (adjusted $p < 0.05$ and log2FC > 0.25), were submitted to the Enrichr portal (https://maayanlab.cloud/Enrichr/). Hallmark gene sets from the molecular signatures database (MSigDB) were utilized for functional enrichment analysis [14].

Additionally, a protein-protein interaction (PPI) network was constructed using the STRING database [15]. The 109 genes from module 2 were uploaded, and disconnected nodes were eliminated from the network. Visualization of the PPI network was achieved using Cytoscape [16].

8. Survival prognosis analysis for modules

The survival map was characterized using the GEPIA2 portal to assess the overall survival (OS) across five modules (http://gepia2.cancer-pku.cn/) [17]. The shared genes between DEGs of clusters from each module served as inputs for survival analysis, with the group cutoff set at median values. A p-value significance threshold of < 0.05 was applied. Survival analysis was conducted using the Cox proportional hazards model.

9. Identification of candidate drugs

To identify potential drug candidates targeting module 2, we utilized the Drug-Gene Interaction Database (DGIDB) (https://www.dgidb.org/), a comprehensive tool for exploring drug-gene interactions [18]. We uploaded the 18 genes from module 2 into DGIDB and filtered the results to include only Food and Drug Administration (FDA)–approved drugs, ensuring clinical relevance.

Results

1. Pathologic annotation and RNA expression

Regions within the breast were categorized as DCIS, invasive carcinoma, necrosis, tumor stroma, non-tumor stroma, or epithelium (Fig. 2A). The spatial distribution and proportion of labeled spots were visualized for each patient, demonstrating that DCIS was present only in patient 1 (Fig. 2B). Utilizing these pathological annotations, spatial transcriptome datasets from the three patients were integrated and visualized using a uniform manifold approximation and projection (UMAP) plot (Fig. 2C). Invasive cancer cells were distinctly separated from adjacent stroma, except in spots identified as DCIS and necrosis. These cancer cells were found to express genes, including *PRAME* and *ETV7*, which are known to be highly enriched in TNBC (Fig. 2D). Additionally, the DEGs in the tumor stroma identified genes associated with epithelial-mesenchymal transition (EMT) and tumor progression, such as *COL10A1* and *MMP13*.

Regional categories of BM included invasive carcinoma, necrosis, tumor stroma, and hemorrhage, similar to those

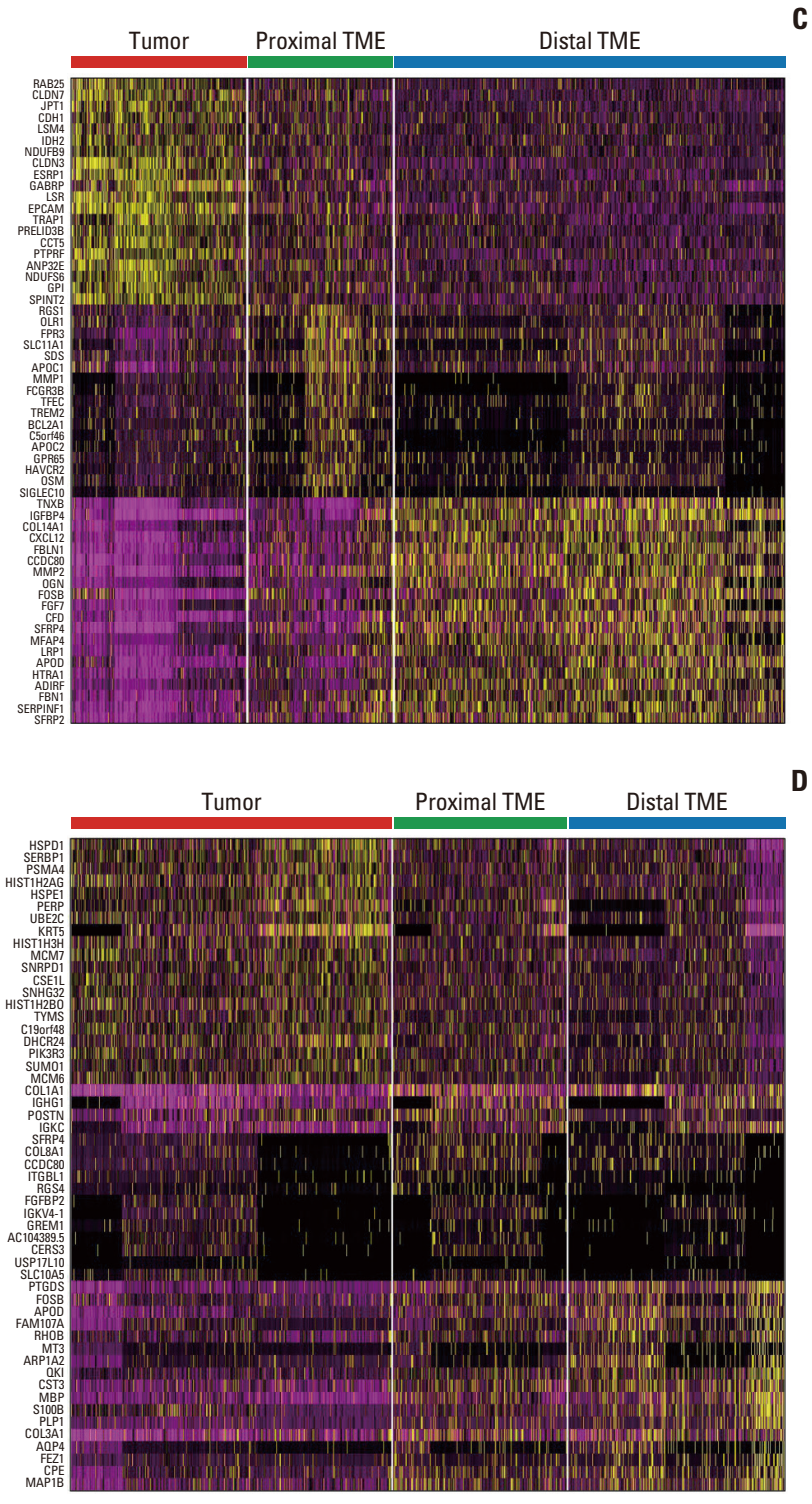

Fig. 3. *(Continued from the previous page)* (C) Heatmap of the top 20 differentially expressed genes from each region in primary triple-negative breast cancer samples. (D) Heatmap of the top 20 differentially expressed genes from each region in brain metastasis samples. *(Continued to the next page)*

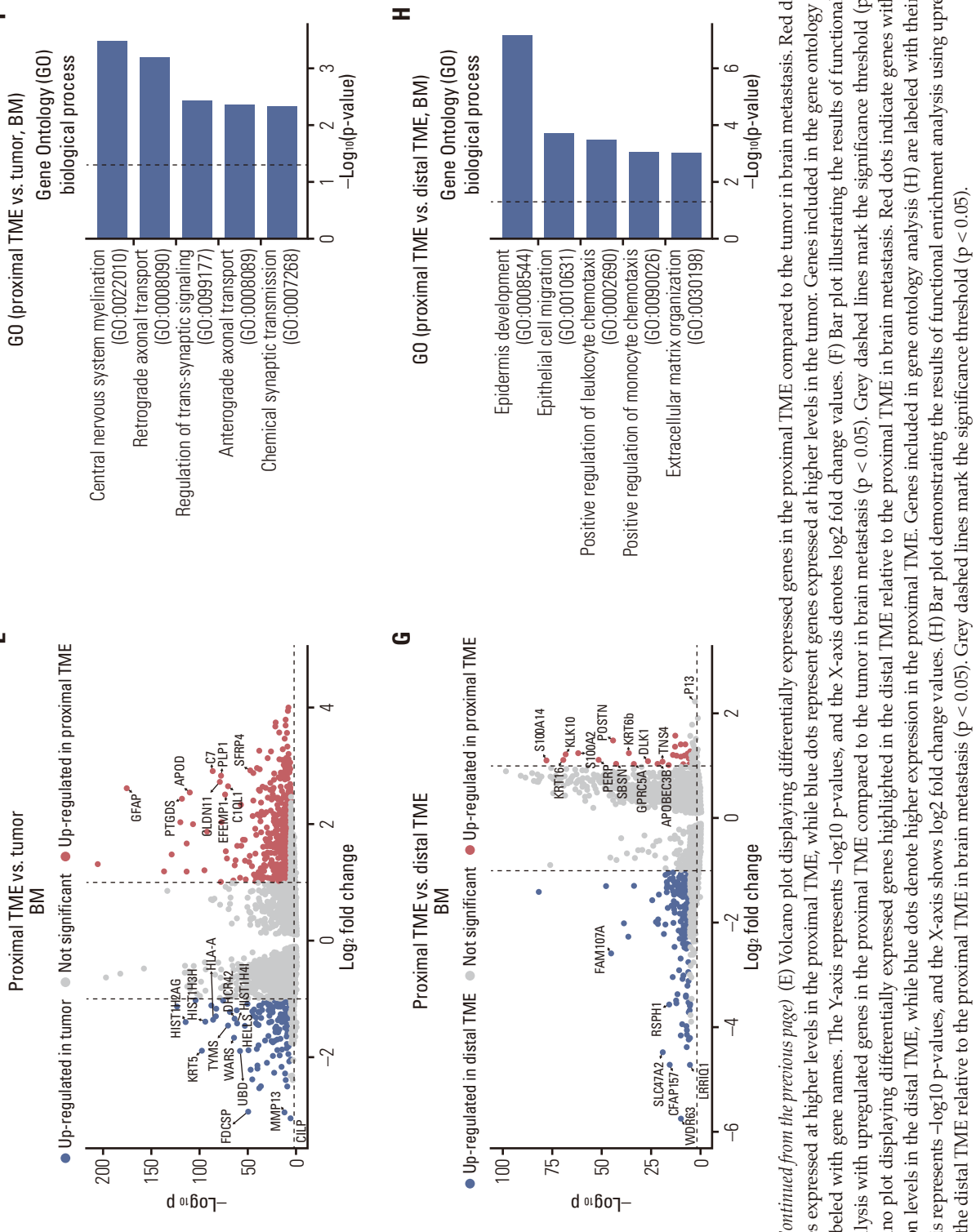

Fig. 3. *(Continued from the previous page)* (E) Volcano plot displaying differentially expressed genes in the proximal TME compared to the tumor in brain metastasis. Red dots indicate genes expressed at higher levels in the proximal TME, while blue dots represent genes expressed at higher levels in the tumor. Genes included in the gene ontology analysis (F) are labeled with gene names. The Y-axis represents –log10 p-values, and the X-axis denotes log2 fold change values. (F) Bar plot illustrating the results of functional enrichment analysis with upregulated genes in the proximal TME compared to the tumor in brain metastasis ($p < 0.05$). Grey dashed lines mark the significance threshold ($p < 0.05$). (G) Volcano plot displaying differentially expressed genes highlighted in the distal TME relative to the proximal TME in brain metastasis. Red dots indicate genes with higher expression levels in the distal TME, while blue dots denote higher expression in the proximal TME. Genes included in gene ontology analysis (H) are labeled with their names. The Y-axis represents –log10 p-values, and the X-axis shows log2 fold change values. (H) Bar plot demonstrating the results of functional enrichment analysis using upregulated genes in the distal TME relative to the proximal TME in brain metastasis ($p < 0.05$). Grey dashed lines mark the significance threshold ($p < 0.05$).

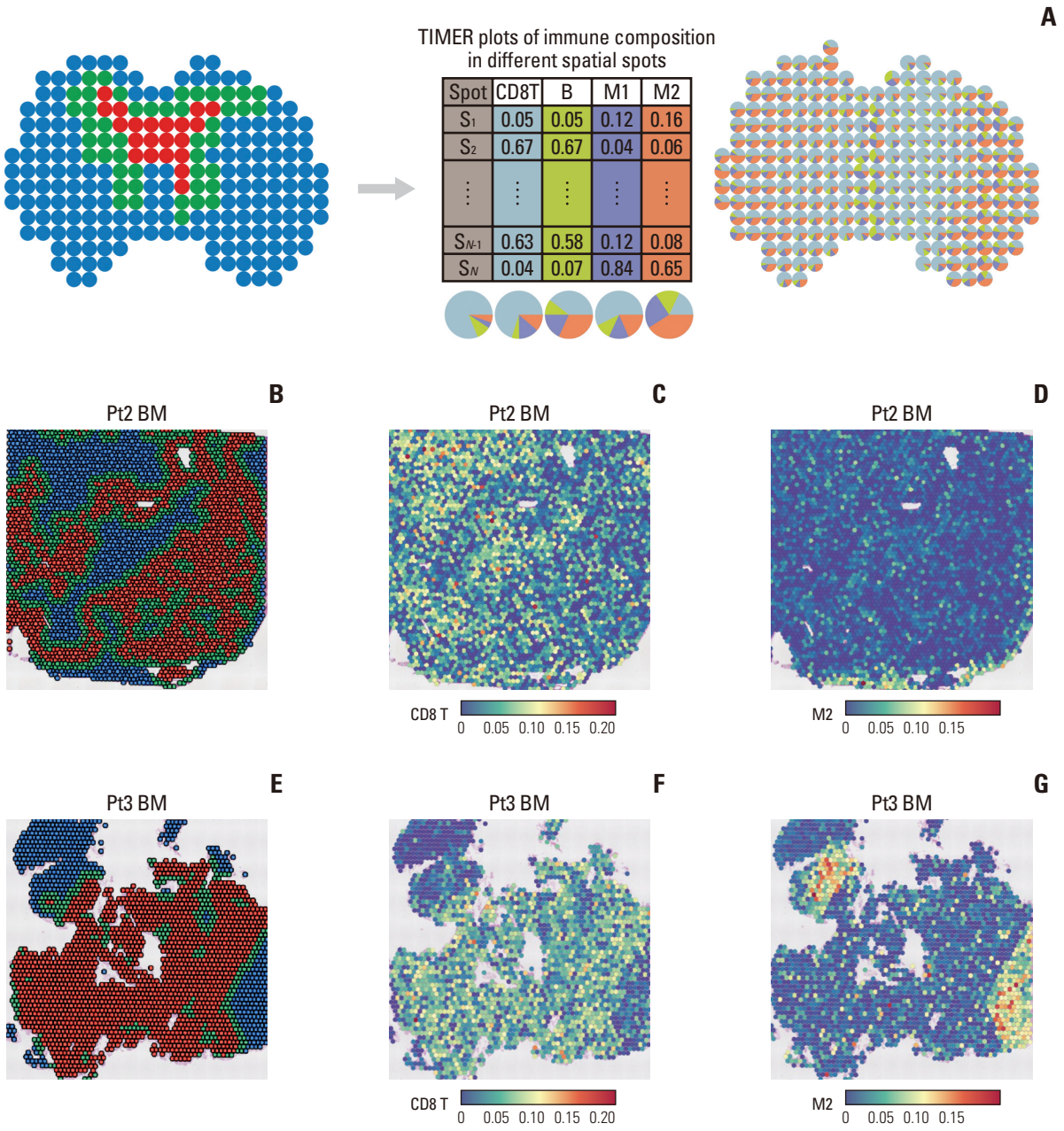

Fig. 4. Spatial visualization and quantification of immune cells using TIMER. (A) Schematic figure depicting the method used to calculate immune cell infiltration in each spot employing TIMER. (B) The distribution of the tumor, proximal tumor microenvironment (TME), and distal TME in the brain metastases (BM) of patient 2. (C) The distribution of CD8+ T cells, calculated using TIMER, in the BM of patient 2. (D) The distribution of M2 macrophages, determined using TIMER, in the BM of patient 2. (E) The distribution of the tumor, proximal TME, and distal TME in the BM of patient 3. (F) The distribution of CD8+ T cells, calculated using TIMER, in the BM of patient 3. (G) The distribution of M2 macrophages, calculated using TIMER, in the BM of patient 3. *(Continued to the next page)*

of PC tissue except for the absence of DCIS and non-tumor stroma (Fig. 2E and F). The UMAP displayed closely located areas of necrosis and invasive carcinoma, reflecting their shared molecular features (Fig. 2G). Meanwhile, tumor stroma and hemorrhage formed distinct clusters from invasive carcinoma. A heatmap of the DEGs revealed that invasive carcinoma expressed genes associated with breast cancer BM, such as *KRT5* and *GBP1*, compared to the tumor stroma (Fig. 2H). DEG analysis between tumor tissues from BM and PC revealed significant transcriptional differences. Several

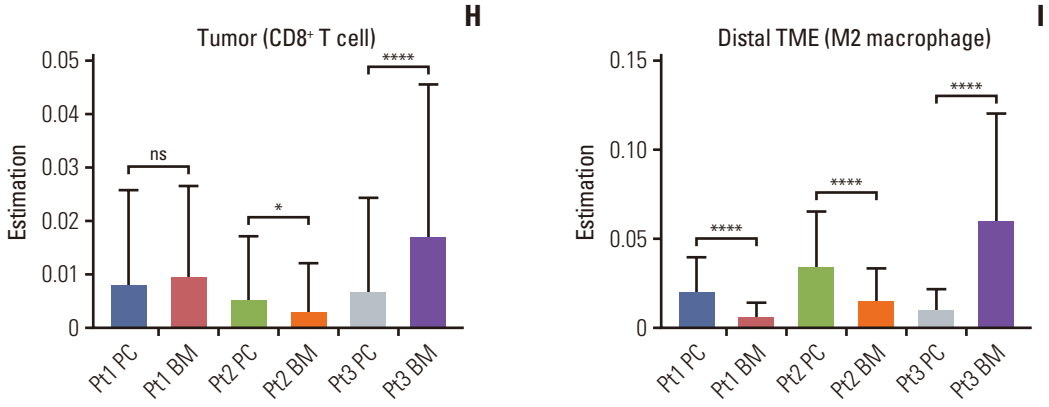

Fig. 4. *(Continued from the previous page)* (H) A bar plot showing the estimated values of CD8+ T cells within the tumor regions in each sample. (I) A bar plot showing the estimated values of M2 macrophages within the distal TME regions in each sample. PC, primary breast cancer. *$p < 0.05$, ****$p < 0.0001$; ns, not significant.

genes were markedly upregulated in PC compared to BM, with *PIGR*, *CCL11*, and *CCL21* showing the highest expression levels. Other notable genes included *COL6A6*, *LRRC15*, *TAC1*, and *CD1C*, along with immunoglobulin-related genes such as *IGHV6-1*, *IGHA1*, and *JCHAIN*. Conversely, multiple genes were significantly upregulated in BM compared to PC. Among them, *MAGEA10*, *DCD*, and *FTHL17* exhibited the highest differential expression. Additionally, *GFAP* and *SLC18A3*, genes associated with neural and glial function, were enriched in BM. Other significantly upregulated genes, including *ARG1*, *SPPL2C*, *LY6L*, and *GRM3*, suggest potential adaptations of metastatic tumor cells to the brain microenvironment (S1 Fig.). These findings confirm the accuracy and specificity of the pathological annotation of each spatially defined region.

2. Tumor-proximity TME analysis

We analyzed the transcriptomic profiles of peritumoral and non-tumor regions in relation to the tumor across paired primary and BM samples. Non-tumor spots were categorized into proximal and distal groups (referred to as proximal and distal TMEs) based on their distance from the tumor, with ≤ 120 μm defined as proximal and > 120 μm as distal (Fig. 3A). These criteria were superimposed on the H&E image, as shown in Fig. 3B. In PC samples, these three regions displayed distinct transcriptional profiles (Fig. 3C). The expression of TNBC-specific tumor genes, such as *RAB25* and *CLDN7*, progressively decreased from the proximal to the distal TME. Interestingly, matrix metalloproteinase (MMP) family members exhibited differential expression between the proximal and distal TME. MMP1 increased while MMP2 decreased in the proximal TME, in line with MMP1's involvement in extracellular matrix remodeling supportive of cancer invasiveness and metastasis. In contrast, this expression pattern was reversed in the distal TME, where genes commonly expressed in the fibroblasts of normal breast stroma such as *TNXB*, *COL14A1*, and *FBLN1* were predominantly expressed. Region-specific expression was less evident in brain metastasis samples; however, the proximal TME of BM was still differentiated from the tumor, characterized by the expression of neuronal genes involved in myelination and axonal transport, including *GFAP*, *PLP1*, *APOD*, *SFRP4* and *CLDN11* (Fig. 3D-F, S2 Fig.). Compared to the distal TME, the proximal TME in these samples prominently expressed genes typically found in epithelial tissues, such as *S100A14*, *S100A2*, *KRT16*, *KRT6B*, *KLK10*, and *POSTN*, which are normally absent in the healthy brain (Fig. 3G and H, S3 Fig.).

3. Deconvolution

The TIMER algorithm was used to estimate the infiltration of immune cells by zone, specifically targeting CD8+ T cells, regulatory T cells, M1 macrophages, and M2 macrophages (S4 Fig.). The analysis scheme is depicted in Fig. 4A. Fig. 4B and E demonstrate the estimated zonal distribution of immune cells in the BM of patient 2 and patient 3, respectively. Spatial heatmaps visualize the relative infiltration of CD8+ T cells and M2 macrophages in patient 2 (Fig. 4C and D) and patient 3 (Fig. 4F and G). In the tumor region, the estimation of CD8+ T cells showed a significantly higher rate in the BM compared to the PC in patient 3, who underwent immunotherapy, than in patients 1 and 2, who were treated with conventional chemotherapy ($p < 0.001$) (Fig. 4H). Notably, in the spatial context for patient 2, there was no increase in CD8+ T cell estimation within the tumor region; rather, an increase was noted in the distal TME. Conversely, in patient 3, an increase in CD8+ T cells was observed in the tumor

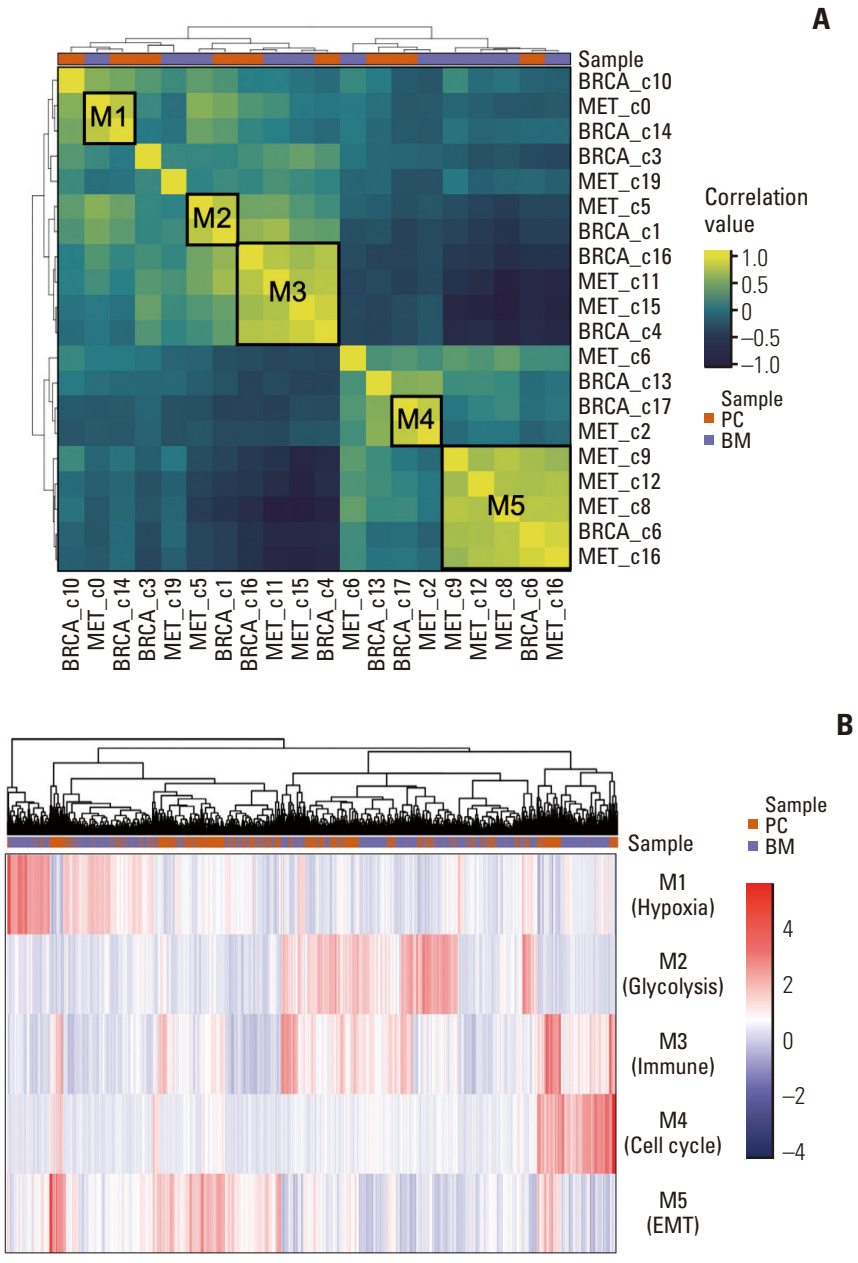

Fig. 5. Core gene signature associated with brain metastasis in triple-negative breast cancer. (A) Heatmap showing the correlation of 20 spatial cluster signatures from different samples indicated by various colors at the top. Hierarchical clustering identified five modules comprising clusters from primary breast cancer (PC) and brain metastasis (BM). (B) Heatmap of the five modules, each characterized by distinct expression patterns across all integrated datasets. Each module is labeled based on the results of functional enrichment analysis.
(Continued to the next page)

region (Fig. 4F and H). In the distal TME region, the estimation of M2 macrophages showed a decreased pattern in the BM compared to the PC in patients 1 and 2, while a significant increase was observed in patient 3 ($p < 0.001$) (Fig. 4I). A detailed regional distribution of different immune cells is presented in S4 Fig.

4. Tumor-specific modules and clinical relevance

To identify the core transcriptional signatures associated with BM in three patients, we first derived DEGs from cancer clusters found in primary and metastatic breast cancer datasets. Genes common to multiple clusters were excluded, and clusters with fewer than 50 DEGs were omitted from

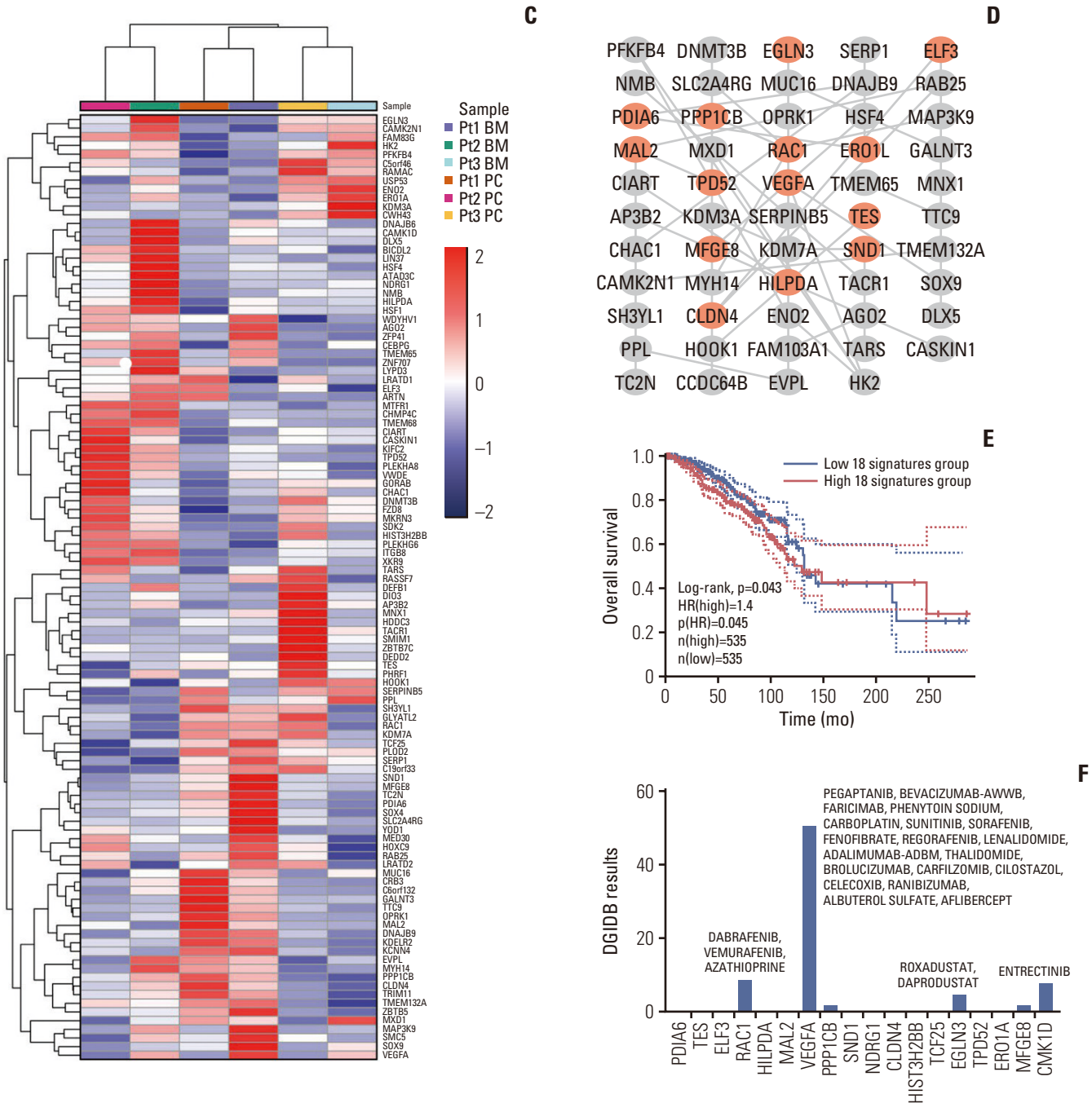

Fig. 5. *(Continued from the previous page)* (C) Heatmap displaying gene expression levels for 109 genes in module 2, with the top annotation bar employing various colors to differentiate longitudinal samples from three patients. (D) A protein-protein interaction network showcasing 14 hub genes from the 109 genes in module 2, with orange nodes representing hub genes. (E) Survival analysis for a breast cancer cohort conducted using GEPIA2. Kaplan-Meier curves for the 18 gene signatures of module 2 (Glycolysis) reveal differences in overall survival between groups. (F) Identification of drug candidates interacting with the 18 genes in module 2 via Drug-Gene Interaction Database (DGIDB). EMT, epithelial-mesenchymal transition; HR, hazard ratio.

the analysis. We selected 20 clusters (9 from PC and 11 from BM) for integration. Hierarchical clustering and correlation analysis were applied to identify significant modules based on a correlation coefficient threshold of $R > 0.6$ (Fig. 5A). Five modules were confirmed, enriched with genes involved in hypoxia, glycolysis, immune response, cell cycle regulation, and EMT (Fig. 5B). Among them, the glycolysis-related program (M2) comprising 109 significant genes showed high expression across the six samples ($p < 0.05$ and average log2FC > 0.25) (Fig. 5C). To identify hub genes within M2, we constructed a PPI network using the 109 genes as nodes via the STRING database. Fourteen hub genes were identified in the network, overlapping with an 18-gene list based on adjusted $p < 0.05$ in M2 (Fig. 5D). Kaplan-Meier survival analysis revealed that these 18 genes in module M2 (adjusted $p < 0.05$ and average log2FC > 0.25) significantly impacted survival outcomes in the breast cancer cohort of The Cancer Genome Atlas (TCGA)/Genotype-Tissue Expression (GTEx) data, with a hazard ratio of 1.4 and a p-value of 0.045 (Fig. 5E). To identify potential drug candidates targeting the 18 genes in M2, we conducted drug repurposing analysis using the DGIDB database, validated as an effective drug screening tool. The analysis identified 25 potential drug candidates associated with four genes: *VEGFA*, *RAC1*, *EGLN3*, and *CAMK1D* (Fig. 5F).

Discussion

Despite decades of research aimed at understanding the molecular basis of BM in breast cancer, the underlying mechanisms remain unclear, and treatment outcomes are still poor. Single-cell technologies have revolutionized the field by providing high-resolution insights into various cellular phenotypes based on gene expression but have lacked spatial information. In this study, we employed spRNA-seq to analyze residual tumor in post-treated TNBC and paired BM tissues, aiming to investigate the biological nature of tumors across different sites and the molecular alterations in the adjacent non-tumor area at metastatic sites. Through zonal categorization based on proximity to tumor regions, we identified transcriptional differences in the TME, focusing on immune-related genomic features.

The proximal TME of BM exhibited heightened activity in central nervous system processes, such as myelination and trans-synaptic signaling compared to the tumor epicenter, thereby indirectly suggesting neuron-tumor interactions at the tumor margin. Venkataramani et al. [19] demonstrated that excitatory synapses form between neuronal cells and cells of metastatic melanoma and breast cancer. Additionally, Zeng et al. [20] reported that activation of the N-methyl-D-aspartate receptor by glutamate ligands is linked with poor prognosis in cancer. Similarly, we noted upregulation of *GRIA4* (glutamate ionotropic receptor AMPA type subunit 4) in the proximal TME, providing additional clinical evidence that synaptic molecule upregulation may facilitate the colonization of metastatic TNBC cells in the brain.

The introduction of ICB has profoundly transformed systemic treatment approaches for various solid tumors. Within breast cancer, TNBC is identified as the subtype most likely to benefit from ICBs, owing to its relatively higher immunogenicity [21]. The IMpassion130 trial has established atezolizumab in combination with nab-paclitaxel as the preferred first-line treatment for patients with advanced TNBC who are PD-L1–positive (SP-142 ≥ 1% in immune cells) [22]. Elevated TILs level have been associated with improved responses to anti–PD-1/PD-L1 therapies in metastatic TNBC. In the IMpassion130 trial, patients with PD-L1 positivity and TILs ≥ 10% exhibited better progression-free survival and OS. The phase III KEYNOTE-119 trial further confirmed the superior therapeutic effect of pembrolizumab in metastatic TNBC patients with TILs ≥ 5% [21]. These findings are consistent with earlier results from the phase II KEYNOTE-086 trial and previous phase I studies [23,24]. Although high TILs level is a robust predictor of ICB response, evidence on whether ICBs directly enhance TILs levels in addition to reinvigorating their function remains limited [25]. In our study, longitudinal tissue analysis revealed increased CD8+ T cell infiltration in the BM following ICB therapy in patient 3, relative to breast cancer tissue collected before ICB treatment. However, conventional chemotherapy did not seem to recruit CD8+ T cells in patients 1 and 2. Further studies involving larger patient cohorts are needed to confirm the activation of systemic T cell responses following ICB treatment. Additionally, as immune cell distribution may be influenced by factors such as PD-L1 expression and other immune profiles, further investigation is necessary to elucidate these interactions.

We also identified core transcriptional programs common to both primary and metastatic breast cancer, including those associated with glycolysis, immune response, cell cycle, and EMT. Among these, key genes in the glycolysis-related module, such as *VEGFA* and *RAC1*, were linked to poorer OS in the breast cancer cohort of the TCGA/GTEx data. Previous studies have shown that breast cancer cells undergo metabolic reprogramming during EMT, increasing glycolysis and lipid metabolism to enhance their invasiveness [26]. While luminal subtypes display either the reverse Warburg effect or a null phenotype, TNBCs predominantly rely on glycolysis [27]. Furthermore, the upregulation of key glycolytic enzymes, such as *HK2* and glucose transporter 3, has been observed in BM [28,29], indicating that glycolysis may serve as an alternative energy source to support the colonization

and survival of metastatic cancer cells in the brain.

spRNA-seq has inherent limitations in deriving detailed cellular conclusions. Unlike scRNA-seq, it does not enable direct analysis of cell-to-cell interactions, identification of subpopulations within specific cell types, or measurement of dynamic cellular changes. However, its key strength lies in its ability to quantitatively assess spatial relationships between cells and define specific regions based on spatial proximity. Using this approach, we successfully distinguished non-tumor regions based on their distance from tumor spots. Despite the small sample size, we noted a significant genomic difference between the proximal and distal TMEs, highlighting the need for thorough consideration in pathological non-tumor areas. By analyzing the proximal and distal TMEs, we identified two distinct expression patterns relating to neuronal and epithelial genes. Furthermore, employing spot-specific count data for cell deconvolution techniques enables the quantitative analysis of immune cell infiltration. However, the spatial resolution of Visium, which utilizes 55-micron spot sizes, offers an average resolution of 1 to 10 cells per spot. This limitation indicates that with Visium data alone, we can only estimate immune cell proportions. To overcome this, platforms such as Xenium *in situ* spatial transcriptomics or multiplex immunohistochemistry could prove beneficial.

This study has several limitations. Firstly, the small number of patients and the heterogeneity in their treatment regimens may limit the generalizability of the findings. Additionally, the analysis was conducted without single-cell resolution, which could diminish the granularity of insights into the TME. Another limitation is the inability to analyze pretreatment biopsy samples, which could have provided valuable baseline information. Finally, the study focused on post-treatment residual disease, and all patients exhibited residual disease following neoadjuvant therapy, suggesting that these patients were already predisposed to poor outcomes, further complicating the interpretation of the results.

In conclusion, we found that the microenvironments of PC and BM can be transcriptionally distinguished based on the relative location of tissue components and their proximity to the tumor. In BM, gene sets related to synaptic connections with neurons may serve as a crucial niche for metastatic tumor cells. Additionally, alterations in immune-related genomic features, driven by ICB, could suggest potential therapeutic options for patients with specific immune profiles. While further research is needed to validate some of our findings, we have contributed to a better understanding of the spatial context within the BM TME.

Electronic Supplementary Material

Supplementary materials are available at Cancer Research and Treatment website (https://www.e-crt.org).

Ethical Statement

This study was approved by the Institutional Review Board of Gangnam Severance Hospital (no. 3-2021-0447), and the requirement for informed consent was waived.

Author Contributions

Conceived and designed the analysis: Yoo J, Kim JH, Cha YJ.
Collected the data: Park I, Park HH, Cha YJ.
Contributed data or analysis tools: Yoo J, Kim HJ, Lee S, Cha YJ.
Performed the analysis: Yoo J, Park I, Kim HJ, Lee S.
Wrote the paper: Yoo J, Kim HJ, Kim JH, Cha YJ.

ORCID iDs

Jihwan Yoo : https://orcid.org/0000-0001-8746-1245
Inho Park : https://orcid.org/0000-0003-2250-6507
Hyun Jung Kim : https://orcid.org/0000-0002-9520-1109
Jee Hung Kim : https://orcid.org/0000-0002-9044-8540
Yoon Jin Cha : https://orcid.org/0000-0002-5967-4064

Conflicts of Interest

Conflict of interest relevant to this article was not reported.

Funding

This research was supported by a National Research Foundation of Korea (NRF) grant funded by the Korean government [grant number: RS-2023-246346, RS-2023-00220894, and NRF-2021R1G-1A1093596]. This research was supported by a grant from the Korea Health Technology R&D Project through the Korea Health Industry Development Institute (KHIDI), funded by the Ministry of Health & Welfare, Republic of Korea [grant number: HI22C2194]. This study was supported by a faculty research grant from Yonsei University College of Medicine (6-2023-0200). This study was supported by a faculty research grant from Gangnam Severance Hospital (D-2023-0002).

Acknowledgments

Spatial transcriptome data were obtained from GENINUS Inc. MID (Medical Illustration & Design), a member of the Medical Research Support Services at Yonsei University College of Medicine, providing excellent support with medical illustration. MID (Medical Illustration & Design), as a member of the Medical Research Support Services of Yonsei University College of Medicine, providing excellent support with medical illustration.

References

1. Ostrom QT, Wright CH, Barnholtz-Sloan JS. Brain metastases: epidemiology. Handb Clin Neurol. 2018;149:27-42.
2. Schouten LJ, Rutten J, Huveneers HA, Twijnstra A. Incidence of brain metastases in a cohort of patients with carcinoma of the breast, colon, kidney, and lung and melanoma. Cancer. 2002;94:2698-705.
3. Kennecke H, Yerushalmi R, Woods R, Cheang MC, Voduc D, Speers CH, et al. Metastatic behavior of breast cancer subtypes. J Clin Oncol. 2010;28:3271-7.
4. Choi JE, Kim Z, Park CS, Park EH, Lee SB, Lee SK, et al. Breast cancer statistics in Korea, 2019. J Breast Cancer. 2023;26:207-20.
5. American Cancer Society. Triple-negative breast cancer [Internet]. American Cancer Society; 2023 [cited 2025 Mar 10]. Available from: https://www.cancer.org/cancer/types/breast-cancer/about/types-of-breast-cancer/triple-negative.html
6. Kwa MJ, Adams S. Checkpoint inhibitors in triple-negative breast cancer (TNBC): where to go from here. Cancer. 2018;124:2086-103.
7. Loi S, Sirtaine N, Piette F, Salgado R, Viale G, Van Eenoo F, et al. Prognostic and predictive value of tumor-infiltrating lymphocytes in a phase III randomized adjuvant breast cancer trial in node-positive breast cancer comparing the addition of docetaxel to doxorubicin with doxorubicin-based chemotherapy: BIG 02-98. J Clin Oncol. 2013;31:860-7.
8. Schmid P, Cortes J, Dent R, Pusztai L, McArthur H, Kummel S, et al. Event-free survival with pembrolizumab in early triple-negative breast cancer. N Engl J Med. 2022;386:556-67.
9. Adams S, Gatti-Mays ME, Kalinsky K, Korde LA, Sharon E, Amiri-Kordestani L, et al. Current landscape of immunotherapy in breast cancer: a review. JAMA Oncol. 2019;5:1205-14.
10. Schmid P, Cortes J, Dent R, McArthur H, Pusztai L, Kummel S, et al. Overall survival with pembrolizumab in early-stage triple-negative breast cancer. N Engl J Med. 2024;391:1981-91.
11. Sun L, Kienzler JC, Reynoso JG, Lee A, Shiuan E, Li S, et al. Immune checkpoint blockade induces distinct alterations in the microenvironments of primary and metastatic brain tumors. J Clin Invest. 2023;133:e169314.
12. Li T, Fu J, Zeng Z, Cohen D, Li J, Chen Q, et al. TIMER2.0 for analysis of tumor-infiltrating immune cells. Nucleic Acids Res. 2020;48:W509-14.
13. Kuleshov MV, Jones MR, Rouillard AD, Fernandez NF, Duan Q, Wang Z, et al. Enrichr: a comprehensive gene set enrichment analysis web server 2016 update. Nucleic Acids Res. 2016;44:W90-7.
14. Liberzon A, Birger C, Thorvaldsdottir H, Ghandi M, Mesirov JP, Tamayo P. The Molecular Signatures Database (MSigDB) hallmark gene set collection. Cell Syst. 2015;1:417-25.
15. Szklarczyk D, Gable AL, Lyon D, Junge A, Wyder S, Huerta-Cepas J, et al. STRING v11: protein-protein association networks with increased coverage, supporting functional discovery in genome-wide experimental datasets. Nucleic Acids Res. 2019;47:D607-13.
16. Shannon P, Markiel A, Ozier O, Baliga NS, Wang JT, Ramage D, et al. Cytoscape: a software environment for integrated models of biomolecular interaction networks. Genome Res. 2003;13:2498-504.
17. Tang Z, Kang B, Li C, Chen T, Zhang Z. GEPIA2: an enhanced web server for large-scale expression profiling and interactive analysis. Nucleic Acids Res. 2019;47:W556-60.
18. Griffith M, Griffith OL, Coffman AC, Weible JV, McMichael JF, Spies NC, et al. DGIdb: mining the druggable genome. Nat Methods. 2013;10:1209-10.
19. Venkataramani V, Karreman MA, Nguyen LC, Tehranian C, Hebach N, Mayer CD, et al. Direct excitatory synapses between neurons and tumor cells drive brain metastatic seeding of breast cancer and melanoma [Preprint]. Posted 2024 Jan 8. bioRxiv https://doi.org/10.1101/2024.01.08.574608
20. Zeng Q, Michael IP, Zhang P, Saghafinia S, Knott G, Jiao W, et al. Synaptic proximity enables NMDAR signalling to promote brain metastasis. Nature. 2019;573:526-31.
21. Brown LC, Salgado R, Luen SJ, Savas P, Loi S. Tumor-infiltrating lymphocytes in triple-negative breast cancer: update for 2020. Cancer J. 2021;27:25-31.
22. Schmid P, Rugo HS, Adams S, Schneeweiss A, Barrios CH, Iwata H, et al. Atezolizumab plus nab-paclitaxel as first-line treatment for unresectable, locally advanced or metastatic triple-negative breast cancer (IMpassion130): updated efficacy results from a randomised, double-blind, placebo-controlled, phase 3 trial. Lancet Oncol. 2020;21:44-59.
23. Adams S, Schmid P, Rugo HS, Winer EP, Loirat D, Awada A, et al. Pembrolizumab monotherapy for previously treated metastatic triple-negative breast cancer: cohort A of the phase II KEYNOTE-086 study. Ann Oncol. 2019;30:397-404.
24. Adams S, Loi S, Toppmeyer D, Cescon DW, De Laurentiis M, Nanda R, et al. Pembrolizumab monotherapy for previously untreated, PD-L1-positive, metastatic triple-negative breast cancer: cohort B of the phase II KEYNOTE-086 study. Ann Oncol. 2019;30:405-11.
25. Brummel K, Eerkens AL, de Bruyn M, Nijman HW. Tumour-infiltrating lymphocytes: from prognosis to treatment selection. Br J Cancer. 2023;128:451-8.
26. Liu B, Zhang X. Metabolic reprogramming underlying brain metastasis of breast cancer. Front Mol Biosci. 2022;8:791927.
27. Choi J, Kim DH, Jung WH, Koo JS. Metabolic interaction between cancer cells and stromal cells according to breast cancer molecular subtype. Breast Cancer Res. 2013;15:R78.
28. Kuo MH, Chang WW, Yeh BW, Chu YS, Lee YC, Lee HT. Glucose transporter 3 is essential for the survival of breast cancer cells in the brain. Cells. 2019;8:1568.
29. Palmieri D, Fitzgerald D, Shreeve SM, Hua E, Bronder JL, Weil RJ, et al. Analyses of resected human brain metastases of breast cancer reveal the association between up-regulation of hexokinase 2 and poor prognosis. Mol Cancer Res. 2009;7:1438-45.